THESIS FOR THE DEGREE OF LICENTIATE OF ENGINEERING

Reverberation Chamber Characterizations for Passive and Active OTA Measurements

Xiaoming Chen

CHALMERS

Department of Signals and Systems
Antenna Group
Chalmers University of Technology
SE-41296 Göteborg, Sweden

Göteborg, 2010

Reverberation Chamber Characterizations for Passive and Active OTA Measurements

Xiaoming Chen

Technical report No. R011/2010.
ISSN 1403-266X

Department of Signals and Systems
Antenna Group
Chalmers University of Technology
SE-412 96 Göteborg, Sweden
Telephone: +46 (0) 31 772 1000

Contact information:
Xiaoming Chen
Department of Signals and Systems
Chalmers University of Technology
Hörsalsvägen 11
S-412 96 Göteborg
Sweden
Telephone +46 (0)31 772 1934
Email: xiaoming.chen@chalmers.se

Printed in Sweden by Chalmers Reproservice
Göteborg, September, 2010

To my family

Reverberation Chamber Characterizations for Passive and Active OTA Measurements

XIAOMING CHEN
Department of Signals and Systems
Chalmers University of Technology

Abstract

Reverberation chamber (RC) has drawn more and more attention as a multipath emulator over the past decade. It has been used for antenna efficiency measurements. It has also been used to measure diversity gain and multi-input multi-output (MIMO) capacity using multi-port antennas. Apart from the passive measurements mentioned above, RC is able to measure active devices, such as total radiated power (TRP) and total isotropic sensitivity (TIS) for mobile phones, throughputs of wireless local network (WLAN) systems, and so on. All these measurements can be called over-the-air (OTA) measurements.

For active OTA measurements, it is of importance to know under which channel condition the bit error rate (BER) is measured. Parameters that are used to characterize channel in multipath environments are coherence bandwidth, delay spread, coherence time, Doppler spread, coherence distance and angular spread. To determine any of these parameters involves channel sounding. In a normal RC, angular of arrival distribution is almost uniform. The corresponding coherence distances for different antennas can be derived at ease based on the a priori knowledge of uniform angular distribution. Therefore, the task of channel sounding in RC is to determine coherence bandwidth, RMS delay spread, coherence time and Doppler spread. These are studied in papers [A-C].

For passive small single-port antenna measurements, radiation efficiency and mismatch factor are of interest. For multi-port antennas used in multipath environments, correlation, embedded radiation efficiency, diversity gain and MIMO capacity, which are usually used to characterize diversity and MIMO performances of the multi-port antennas, are of interest. All of these can also be measured in RC. Papers concerning these are [D-F].

For active OTA measurements, we need to have an accurate estimation of the power level (path loss) of the RC. For radiation efficiency measurements, the accuracy of the power levels directly determines the accuracy of the measured efficiency. Therefore, it is important to characterize the accuracy of the average power transfer function measured in RC. The average power transfer function is basically power transfer function averaged over all samples. A large number of independent samples ensure good accuracy. However, the maximum number of independent samples for a RC is physically limited by the shape and size of the RC, and the mode-stirrers inside the RC. Thus, the aim of this work is to improve the RC's accuracy. Papers [G-H] are about this work, of which Paper [G] describes how the direct coupling between transmit and receive antennas causes a residual error that is strongly affected by the loading of the chamber.

Keywords: Reverberation chamber, channel sounding, coherence bandwidth, delay spread, Doppler spread, antenna efficiency, diversity, power transfer function.

Contents

List of papers

A. K. Karlsson, X. Chen, P.-S. Kildal and J. Carlsson, “Doppler spread in reverberation chamber predicted from measurements during step-wise stationary stirring”, *IEEE Antennas and Wireless Propagation Letters*, vol. 9, pp. 497-500, 2010.

B. Xiaoming Chen, Per-Simon Kildal, Charlie Orlenius and Jan Carlsson, "Channel sounding of loaded reverberation chamber for Over-the-Air testing of wireless devices - coherence bandwidth and delay spread versus average mode bandwidth", *IEEE Antennas and Wireless Propagation Letters*, vol. 8, pp. 678-681, 2009.

C. Xiaoming Chen, Per-Simon Kildal, "Theoretical derivation and measurements of the relationship between coherence bandwidth and RMS delay spread in reverberation chamber", *3th European Conference on Antennas and Propagation, EuCAP 2009*, Berlin, Germany, 23-27 March, 2009.

D. Xiaoming Chen, Per-Simon Kildal, "Accuracy of antenna mismatch factor and input reflection coefficient measured in reverberation chamber", *3th European Conference on Antennas and Propagation, EuCAP 2009*, Berlin, Germany, 23-27 March, 2009.

E. J. Yang, S. Pivnenko, T. Laitinen, J. Carlsson, X. Chen, “Measurements of diversity gain and Radiation Efficiency of the Eleven Antenna by sing Different Measurement Techniques,”, *4th European Conference on Antennas and Propagation, EuCAP 2010*, Barcelona, Spain, 12-16 April, 2010.

F. Jungang Yin, Daniel Nyberg, Xiaoming Chen, Per-Simon Kildal, “Characterization of Multi-port Eleven Antenna for Use in MIMO System”, *IEEE ISWCS 2008*, Reykjavik, Iceland, Oct. 2008.

G. Per-Simon Kildal, Sz-Hau Lai, and Xiaoming Chen, “Direct Coupling as a Residual Error Contribution during OTA Measurements of Wireless Devices in Reverberation Chamber”, *IEEE AP-S*, Charleston, USA, June 1-5, 2009.

H. Xiaoming Chen, Per-Simon Kildal, “Frequency-Dependent Effects of Platform and Wall Antenna Stirring on Measurement Uncertainty in Reverberation Chamber”, *4th European Conference on Antennas and Propagation, EuCAP 2010*, Barcelona, Spain, 12-16 April, 2010.

Other related publications by the Author not included in this thesis:

- Jian Yang, Xiaoming Chen, Niklas Wadefalk, Per-Simon Kildal, "Design and realization of a linearly polarized Eleven feed for 1-10 GHz", *IEEE Antennas and Wireless Propagation letters*, vol.8, pp. 64-68. 2009.

- Xiaoming Chen and Per-Simon Kildal, "Relations between coherence bandwidth and average mode bandwidth in reverberation chamber for wireless device measurement", *ISAP 2008*, Taipei, 27-30 October 2008.

- Xiaoming Chen, Per-Simon Kildal, "Comparison of RMS Delay Spread and Decay Time Measured in Reverberation Chamber", *4th European Conference on Antennas and Propagation, EuCAP 2010*, Barcelona, Spain, 12-16 April 2010.

- A.A.H. Azremi, J. Toivanen, T. Laitinen, P. Vainikainen, X. Chen, N. Jamaly, J. Carlsson, P.-S Kildal, S. Pivnenk, "On Diversity Performance of Two-Element Coupling Element Based Antenna Structure for Mobile Terminal", *4th European Conference on Antennas and Propagation, EuCAP 2010*, Barcelona, Spain, 12-16 April 2010.

Preface

This report is a thesis for the degree of licentiate of engineering at Chalmers University of Technology. The work is divided into three main parts: channel soundings for active mobile phone measurements, diversity and capacity measurements of multi-port antenna, and accuracy characterization of passive antenna measurements, all in reverberation chamber. This work has been supported in part by the Swedish Governmental Agency for Innovation Systems (VINNOVA) within the VINN Excellence Centre Chase at Chalmers. My main supervisor is Prof. Per-Simon Kildal; my additional supervisors are Prof. Jan Carlsson and Associate Prof. Jian Yang. Per-Simon Kildal is also the examiner. The work was carried out between January 2008 and August 2010 at antenna group of Chalmers.

Acknowledgement

The work in this thesis has been supported by The Swedish Governmental Agency for Innovation Systems (VINNOVA) within the VINN Excellence Center Chase.

First of all I would like to thank my supervisor and examiner Prof. Per-Simon Kildal for accepting me into his group. We had many fruitful discussions. I would also like to thank my secondary supervisor and also my project leader, Prof. Jan Carlsson, for his constant interests and support in my work. Special thanks also go to my additional supervisor, Assoc. Prof. Jian Yang, who is always willing to offer not only numerous technique help but also tremendous help in daily life.

I would like to thank the participants in the MIMO terminals and OTA projects within the Chase VINN Excellence Center, and in particular Chase manager Ingmar Karlsson, for their interest and amicable attitude to my project presentations. Special thanks go to Kristian at SP, and Magnus and Charlie at Bluetest AB, for their technique support.

I would like to thank all colleagues in the antenna group, former as well as present, Daniel, Yogesh, Nima, Ashraf, Elena, Ahmed, Hasan, and our former SPA division members, in particular the division head Prof. Mats Viberg, for creating a nice environment. Appreciation also goes to Prof. Arne Svensson for the same reason. I need to thank Dr. Ulf Carlberg for all kinds of help since I started my PhD studies in the antenna group. I also would like to thank all of my friends, Xuezhi, Tong, Adisak, Yutao, Yiyu, Yiqi …, for making my leisure life blithe.

Last but not least, I would like to thank my wife and parents for their love and support.

1. Introduction

Reverberation chamber (RC) is basically a metal cavity (see Fig. 2.2), which is stirred to emulate a Rayleigh fading environment [1]. The RCs were traditionally used for electromagnetic compatibility (EMC) measurements, but during the past decade it has found new applications for measuring Over-The-Air (OTA) performance of small antenna and wireless devices in multipath environment. It has been used to measure antenna radiation efficiency, diversity gains and capacity of MIMO systems [2]. It can also be used to measure total radiated power [3] and total isotropic sensitivity [4] of active wireless devices and stations. The antenna group at Chalmers University of Technology, together with Bluetest AB, have been world-leading experts in these new fields. Former PhD students at the group, Kent Rosengren, Ulf Carlberg, Kristian Karlsson and Daniel Nyberg have all worked on topics related to RC. This thesis is a further study of RC based on previous knowledge, especially on Kent's works [5].

For active OTA measurements, it is of importance to know under which channel condition the bit error rate (BER) is observed. Parameters that are used to characterize channel in multipath environments are coherence bandwidth, delay spread, coherence time, Doppler spread, coherence distance and angular spread. To determine any of these parameters involves channel sounding. In a normal RC, angular distribution is uniform [6]. The corresponding coherence distances for different antennas can be derived at ease based on the a priori knowledge of uniform angular distribution [7]. Coherence bandwidth and RMS delay spread have been studied in [8]-[10], Doppler spread (with coherence time being inversely proportional to it) in RC is studied in [11].

For passive small single-port antenna measurements, radiation efficiency and mismatch factor are of interest. For multi-port antennas used in multipath environments, correlation, embedded radiation efficiency, diversity gain and MIMO capacity, which are usually used to characterize diversity and MIMO performances of the multi-port antennas, are of interest. All of these parameters can be measured in RC [2], [12]-[15].

For active OTA measurements, we need to have an accurate estimation of the power level (path loss) in the RC. For radiation efficiency measurements, the accuracy of the power levels directly determines the accuracy of the measured efficiency. Therefore, it is important to characterize the accuracy of the power level measured in RC. The power level is basically average power transfer function averaged over all samples. A large number of independent samples ensure good accuracy. However, the maximum number of independent samples for a RC is physically limited by the shape and size of the RC [16], and the mode-stirrers inside the RC [17]. More importantly, it is found that the Rician K-factor in RC [18] represents a residual error for accuracy [19]. As pointed out in [18] that loading the RC (putting more lossy objects in the RC) results in an increased Rician K-factor (residual error), and thereby the accuracy degrades with increasing RC loading [19].

2. RC Channel Sounding

The aim of channel sounding in RC is to determine coherence bandwidth, delay spread, coherence time and Doppler spread.

2.1 Coherence Bandwidth and Delay Spread

The coherence bandwidth B_c, is defined, in this thesis, as the frequency range over which the signal correlation function is larger than 0.5, as shown in Fig. 2.1. In the literature, there are other definitions for coherence bandwidth [20]-[22]. For example, instead of 0.5 a threshold of 0.7 (or some other threshold) is used; instead of using correlation of (complex) signal, correlation of envelope of the signal is used; instead of using half bandwidth full bandwidth is used. Relations for different coherence bandwidth are derived in [9]. In this thesis unless specified, coherence bandwidth means half bandwidth coherence bandwidth based on signal correlation with threshold of 0.5, as shown in Fig. 2.1.

The RC in use here is Bluetest HP reverberation chamber (see Fig. 2.2) with dimensions of 1.8 m x 1.75 m x 1.25 m. The mechanical stirring is performed by two metal plates that are moved stepwise. The platform stirring [25] is realized by a stepwise rotating platform upon which the antenna under test (AUT) is mounted, and polarization stirring [26] is achieved by three antennas mounted on three orthogonal walls. A vector network analyzer (VNA) is used to measure the transfer functions as shown in Fig. 2.2. The frequency response (transfer function) of the channel is a function of frequency and stirrer position, denoted as $H(f,n)$. The complex auto-correlation function (ACF) $R_f(\partial f)$ of the transfer function is

$$R_f(\partial f) = E[H^*(f,n)\cdot H(f+\partial f,n)] / E[|H(f,n)|^2] \tag{2.1}$$

where E denotes expectations. In practice ACF is often evaluated by integrating the product over a frequency band, but then we will not be able to see any possible frequency variations. Therefore, we have chosen to take the expectation over all the stirrer positions n in the reverberation chamber, each one corresponding to an independent realization of the channel. To gather many channel realizations will be very time-consuming when performing measurements in real-life multipath environments, but in the reverberation chamber it is feasible.

The time dispersive properties of multipath channels are usually characterized by their RMS delay spread [23]

$$\sigma_\tau = \sqrt{\sum_k P(\tau_k)\tau_k^{\,2} / \sum_k P(\tau_k) - [\sum_k P(\tau_k)\tau_k / \sum_k P(\tau_k)]^2}$$
$$P(\tau) = |h(\tau)|^2 \tag{2.2}$$

where the received power $P(\tau_k)$ at time delay τ_k is the so-called power delay profile (PDP), and $h(\tau)$ is the impulse response obtained from inverse Fourier transform (IFFT) of the channel frequency response $h(\tau,n) = IFFT\{H(f,n)\}$ at each stirrer position n. RMS delay spread is calculated by (2.2) using PDP averaged over all the stirrer positions.

Delay spread σ_τ and coherence bandwidth B_c are inversely proportional to each other. It is derived in [9]

$$B_c = \sqrt{3} / (2\pi\sigma_\tau) \tag{2.3}$$

Note that (2.3) holds for the coherence definition illustrated in Fig. 2.1 in isotropic scattering environments.

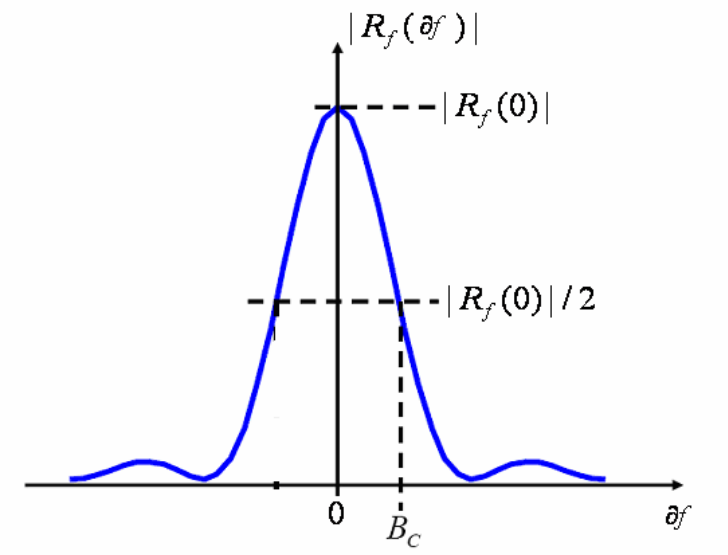

Figure 2.1: Illustration of coherence bandwidth based on signal correlation function.

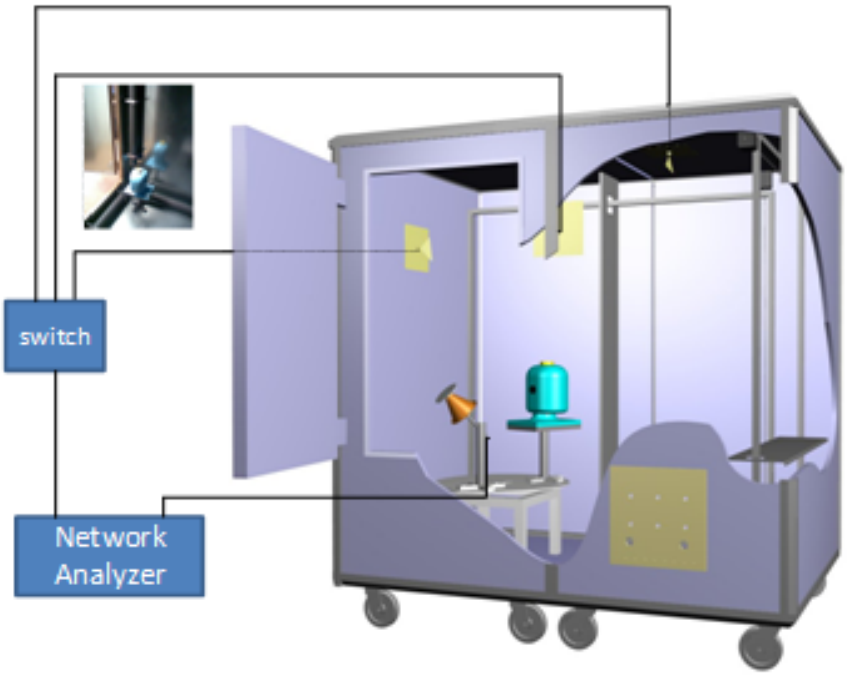

Figure 2.2: Drawing of Bluetest RC with two mechanical plate stirrers, one platform and three wall antennas (The inserted little photo in the upper left corner shows the head phantom and the location of the three absorber-filled PVC cylinders of load2 configuration.)

2.2 Average Mode Bandwidth and Decay Time

The mode bandwidth is defined as the frequency range over which the power in one excited mode is larger than half the power in the mode when it is excited at its resonance frequency. The introduction of average mode bandwidth Δf makes it possible to characterize all the different losses appearing in the reverberation chamber as additive contributions, i.e.

$$\Delta f = \Delta f_{con} + \Delta f_{obj} + \Delta f_{ap} + \Delta f_{ant} \tag{2.4}$$

$$\Delta f_{ant} = \sum_{antennas} c^3 e_{rad} / (16\pi^2 f^2 V) \tag{2.4a}$$

$$\Delta f_{obj} = \sum_{objects} c\sigma_a / (2\pi V) \tag{2.4b}$$

Equation (2.4) is the same as equation (6) in [24], except that it is expressed in terms of $\Delta f = f / Q$ where Q is quality factor of the RC. The different contributions to Δf are Δf_{con} due to finite metallic conductivity, Δf_{obj} due to absorbing objects, Δf_{ap} due to aperture leakage contribution, and Δf_{ant} due to antennas inside the chamber. The detailed formulas for the two dominant contributions Δf_{ant} and Δf_{obj} are given in (2.4a) and (2.4b) respectively, where V is the volume of the chamber, e_{rad} the radiation efficiencies of the antennas, and σ_a the average absorption cross sections of the lossy objects, properly defined in [24]. Equations (2.4a) and (2.4b) are useful in order to understand how Δf is or can be controlled. The average mode bandwidth is given in [24]

$$\Delta f = c_0^3 e_{rad1} e_{rad2} / (16\pi^2 f^2 V G_{ch}) \tag{2.5}$$

where e_{rad1} and e_{rad2} are the total radiation efficiencies of transmitting and receiving antennas in the RC, and G_{ch} is average power transfer function.

From the definition of decay time,

$$\tau_{RC} = Q / \omega = 2\pi\Delta f \tag{2.6}$$

Substitute (2.5) into (2.6), decay time of the RC can be expressed as

$$\tau_{RC} = 8\pi f^2 V G_{ch} / (c_0^3 e_{rad1} e_{rad2}) \tag{2.7}$$

Intuitively the average mode bandwidth should be equal to coherence bandwidth based on their definitions. It is derived in [10] that

$$\sigma_\tau = \sqrt{3}\tau_{RC} \tag{2.8}$$

Average mode bandwidth and coherence bandwidth are calculated and plotted in Fig. 2.3

where “empty” corresponds to unloaded chamber, “loading1” is a head phantom filled with brain equivalent liquid, “loading2” is the head phantom plus three Polyvinyl Chloride (PVC) cylinders filled with microwave absorbers cut in small pieces, and “loading3” is the head phantom plus six such cylinders. The lossy cylinders were located along orthogonal corners of the chamber in such a way that they can be expected to attenuate cavity modes of different polarizations equally much (TE and TM modes), see the photo in the upper left corner of Fig. 2.2. From Fig. 2.3 it is seen that coherence bandwidth and average mode bandwidth are basically the same as expected. Fig. 2.3 shows σ_τ and $\sqrt{3}\tau_{RC}$ measured in RC. It is shown that they agree with each other well for almost all the loadings, especially for loaded RC, over most frequencies.

Compared with coherence bandwidth and RMS delay spread, average mode bandwidth and decay time require less computational efforts. Therefore, they offer a computationally cheaper alternative for channel sounding in RC. In addition, from Fig. 2.3 and Fig. 2.4 it can be seen that the channels in RC can be controlled to emulate flat and frequency-selective fading environments [23], [27] by simply loading the RC.

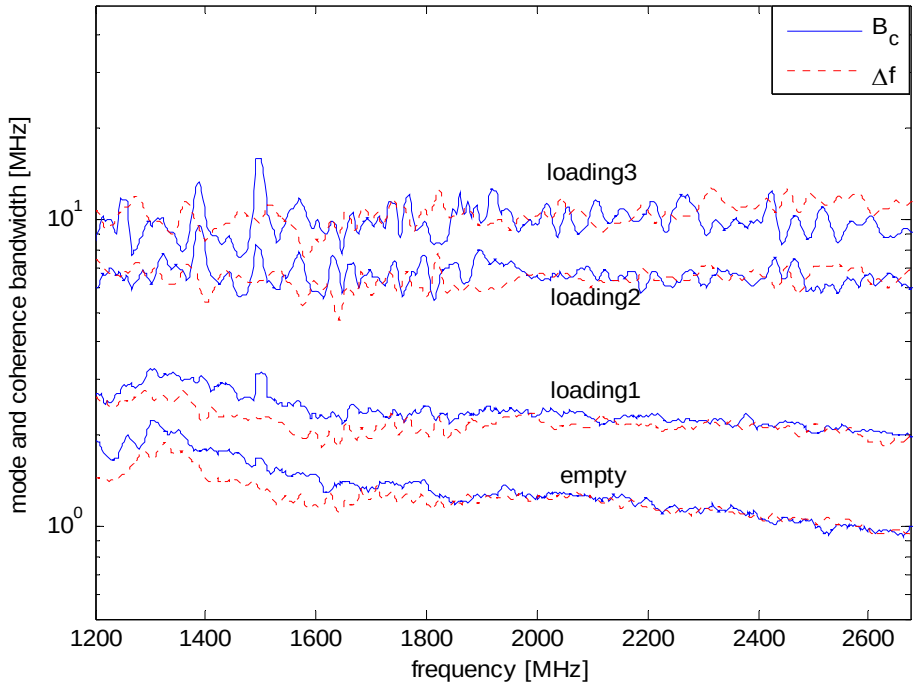

Figure 2.3: Comparison of average mode bandwidths and coherence bandwidths for different loadings of the chamber.

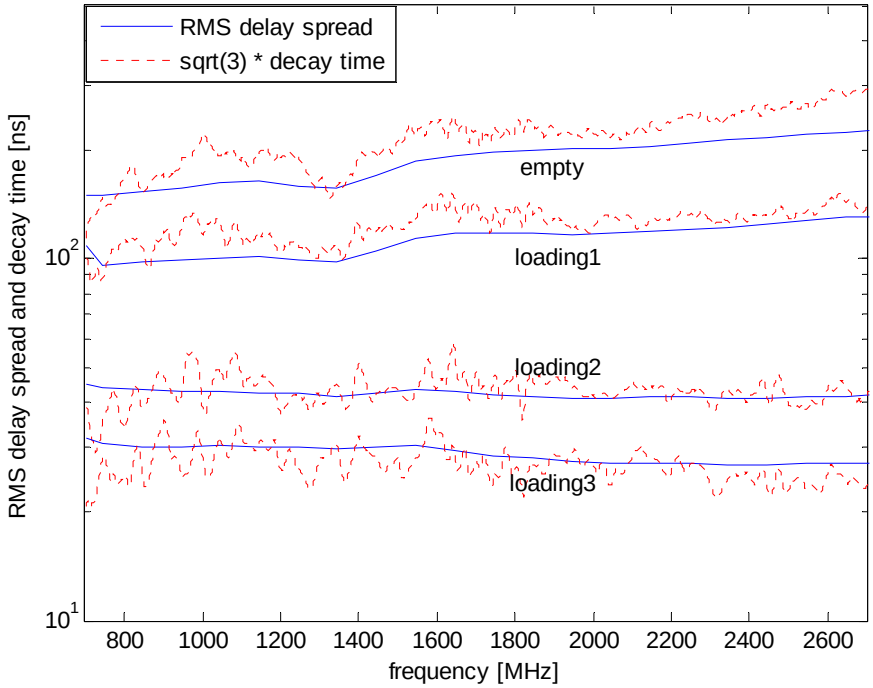

Figure 2.4: Comparison of σ_τ and $\sqrt{3}\tau_{RC}$ in RC for different loadings.

2.3 Doppler Spread

Different methods to determine Doppler spread have been studied [28]-[31]. While [28] and [29] deal with direct evaluation from the formula defining Doppler spread, [30] is mainly dealing with Doppler spread estimation in the presence of carrier frequency offset (CFO). By doing channel sounding in RC with VNA, CFO problem is avoided, and therefore we do not need to resort to sophisticated signal processing algorithm as shown in [30]. Doppler spread in RC has previously been observed by simply sweeping intermediate frequency (IF) bandwidth of VNA in continuous wave mode, and observing the power variation [31]. However, this method gives only a rough estimation of Doppler frequency, and it works for only one single frequency at the time. In this thesis, we will show how the Doppler spread easily can be obtained for assumed stirrer speed even though the measurements themselves are done when the stirrers are stationary. Thus, each VNA measurement is done under stationary conditions with no Doppler shift.

We denote the channel transfer function as a function of frequency and time, $H(f,t)$. Then, its time autocorrelation function is

$$R_H(f,\partial t) = E[H^*(f,t)H(f,t+\partial t)] \tag{2.9}$$

If we now denote ρ the Doppler frequency, the Doppler spectrum becomes [28]

$$D(f,\rho) = \int_{-\infty}^{\infty} R_H(f,\partial t)\exp(-j2\pi\rho\partial t)d(\partial t) \tag{2.10}$$

Doppler spread B_D is defined as the range of Doppler frequency ρ over which $D(f,\rho)$ is above a certain threshold. Note that with $R_H(f,\partial t)$ being complex conjugate symmetric, its Fourier transform $D(f,\rho)$ is real. The autocorrelation function (2.9) is equivalent to

$$R_H(f,\partial t) = H(f,\partial t) \otimes H^*(f,-\partial t) \tag{2.11}$$

where ⊗ represents convolution. Applying Fourier transform to both sides of (2.11), we easily obtain

$$D(f,\rho) = H(f,\rho)H^*(f,\rho) = |H(f,\rho)|^2 \tag{2.12}$$

where $H(f,\rho)$ is the Fourier transform of $H(f,t)$ w.r.t. time t, and the superscript * represents complex conjugation. The channel transfer function is equal to the S-parameter $S_{21}(f,t)$ measured with a VNA corresponding to constant time t along the fading time scale. Such stationary measurements can then be repeated for many different time moments t_n, corresponding to different fixed stirrer positions.

The RC used here is located at SP Technical Research institute of Sweden (SP), which during these measurements makes use of rotating paddle and platform stirring, see Fig. 2.5. The transmitting antenna is a Discone antenna mounted on the platform, and the receiving antenna is a horn directed into a corner of the chamber. The dimensions of the SP RC are: length 3m, width 2.45m and height 2.45m.

The RMS Doppler bandwidth at a certain frequency f_0 is given by

$$\rho_{rms} = \left[\frac{\int \rho^2 D(f_0,\rho)\, d\rho}{\int D(f_0,\rho)\, d\rho} \right]^{1/2} \tag{2.13}$$

The integrations in (2.13) should exclude noise floor (the level where Doppler spectrum becomes flat). Fig. 2.6 shows Doppler spectrum obtained in RC. The step-wise stationary stirring method is described in details in [11]. With this method, Doppler spread can be determined by computation by assuming that the fixed stirrer position steps are the time steps of a continuous movement of the stirrers, and adding a virtual stirrer speed between the positions corresponding to the desired continuous movement of the stirrers. The advantage of this method is that one can obtain Doppler spread with any stirrer speed for the whole sweeping frequency band. To validate the step-wise stationary stirring method, we did measurements during continuously moving stirrers by setting VNA in continuous wave mode at certain frequencies as well. The VNA was used to measure $H(f,t)$ 750 times for one complete rotation of the platform and paddle. The rotation time T was increased to 182 sec in order to be able to capture the data with the data acquisition software, so that the observed Doppler shift was very small. Fig. 2.7 shows the comparison of Doppler spread obtained during continuous stirring and that obtained with step-wise stationary stirring method assuming the same speed. Good agreements are observed.

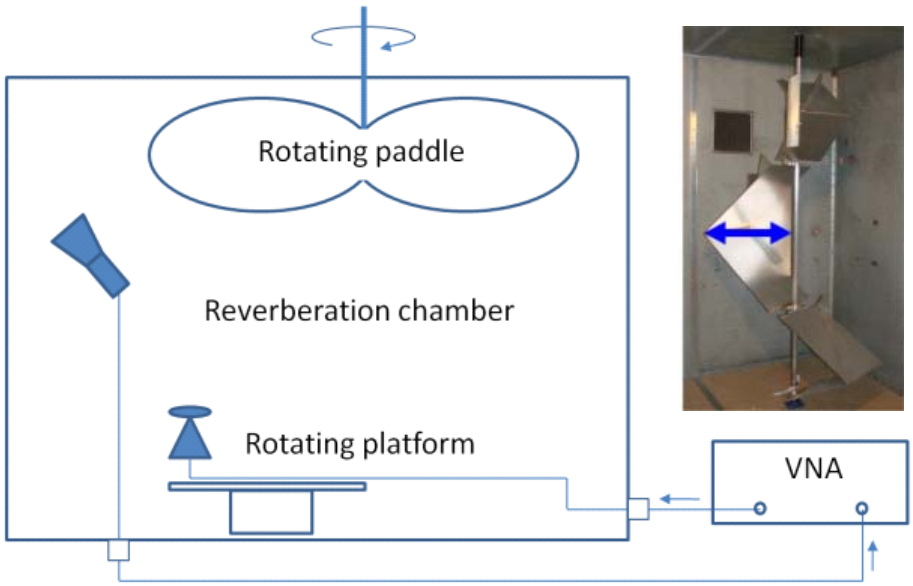

Figure 2.5: Illustration of measurement setup with rotating paddle and platform. The actual mechanical stirrers used in the measurements are shown in photo with its maximum radius specified by the arrow.

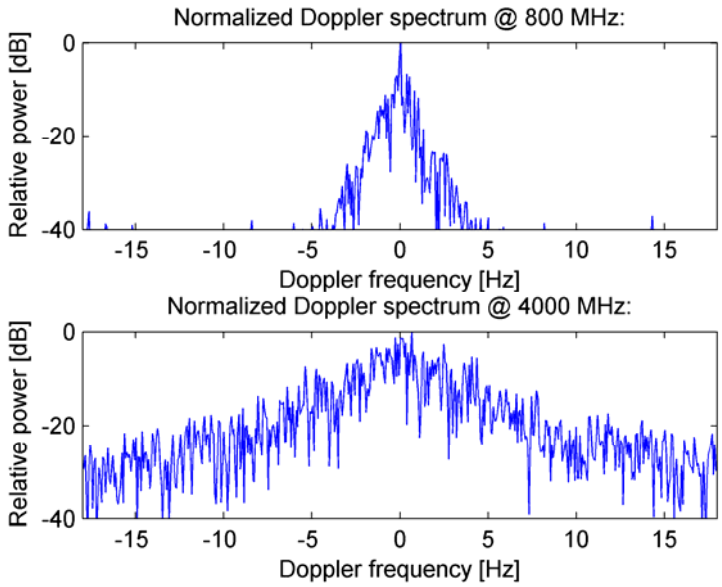

Figure 2.6: Doppler power spectrum at two different frequencies. The RMS Doppler bandwidth for this set of data equal to 1.0 Hz at 800 MHz and 3.6 Hz at 4GHz.

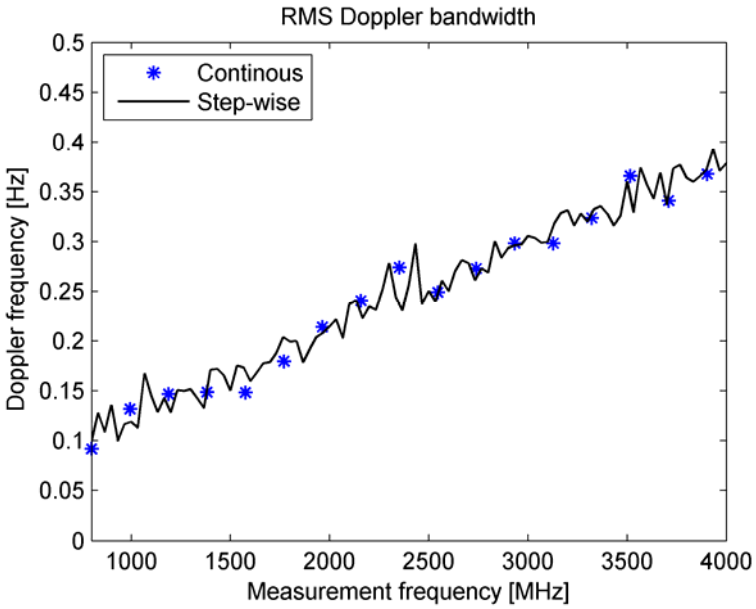

Figure 2.7: Validation of RMS Doppler bandwidth obtained by using present step-wise stationary approach by comparison with results obtained from actual time-varying measurements using continuous movement of the stirrers with given speed at discrete frequencies.

3. Antenna Measurements in RC

The RC can be used to measure radiation efficiency and mismatch factor for single-port antenna, and embedded radiation efficiency, diversity gain and capacity for multi-port antenna. From now on, without specification, RC in use is Bluetest HP reverberation chamber, as shown in Fig. 2.2.

3.1 Measurements of Single-Port Antenna

The radiation efficiency of an antenna under test (AUT) can be measured in RC by the following procedure: first, the average power transfer function of a reference antenna with known radiation efficiency, e_{ref}, is measured as G_{ref}; then, the AUT is measured with another average power transfer function G_{AUT}. The radiation efficiency of the AUT is then

$$e_{rad} = \frac{G_{AUT}}{G_{ref} / e_{ref}} \tag{3.1}$$

The reference antenna in use is a wide band Discone antenna with radiation efficiencies close to unity over its working bandwidth. The power transfer function is pure power level with mismatch factors at both transmitting and receiving sides calibrated out. Therefore, the measurement accuracy of mismatch factor (reflection coefficient) will affect that of the radiation efficiency.

Numerical and statistical models of antenna impedance in cavity have been built in [32], [33]. A common disadvantage of the theoretical models is that they are constrained to linear small antennas with simple geometries. For large antennas with complex geometries and directive patterns, the models are difficult to build. Therefore, the statistical model of measured reflection coefficient proposed in [34] is used in the present paper. Thus, it is assumed that the reflection coefficient can be split into two parts, a free space part and a part coming from the chamber

$$S_{11}^{tot} = S_{11}^{fs} + S_{11}^{RC} \tag{3.2}$$

where S_{11}^{tot} is the total reflection coefficient of the antenna in the chamber measured at its port, S_{11}^{fs} is the free space reflection coefficient that is independent of the RC, and S_{11}^{RC} is the reflection coefficient contribution from the chamber. For a well stirred chamber, S_{11}^{RC} has a zero-mean complex Gaussian distribution [1]. It is clear that S_{11}^{RC} will depend on S_{11}^{fs}, or rather the amplitude free space transmission coefficient of the antenna both when entering the chamber and when leaving it, i.e., in total the power transmission coefficient. Therefore, S_{11}^{RC} is proportional to the mismatch factor, i.e. $1-|S_{11}^{fs}|^2$. The ensemble average of the reflection coefficient measured in the chamber is

$$E[S_{11}^{tot}] = S_{11}^{fs} \tag{3.3}$$

In reality, the number of independent samples in the chamber is always limited, thus, (3.3) is just an approximation. In the thesis, it is shown that with additional complex *frequency* stirring (electronic mode stirring) [35], the estimation accuracy of mismatch factor can be improved.

The AUT is a standard gain horn antenna working from 3.94 to 5.99 GHz (see Fig. 3.1). Measurements were done from 5 to 6 GHz with a frequency step of 1 MHz. For a single frequency, there are 200 stirrer positions (20 platform positions and 10 stirrer plate positions) for each of the three wall antennas. Thus, for a single frequency, there are 600 samples. Fig. 3.2 shows the mismatch factor at one stirrer position in RC and that in anechoic chamber. Fig. 3.3a shows mismatch factor of AUT in RC when S_{11}^{fs} is obtained by complex stirring over positions only, and it is compared with results from anechoic chamber. Fig. 3.4a shows similar results but with additional 100 MHz complex frequency stirring for the reverberation chamber case. The improved accuracy can be explained by the histograms without and with 100 MHz complex frequency stirring, shown in Fig. 3.3b and Fig. 3.4b. With additional complex frequency stirring, the mean value of S_{11}^{RC} approaches zero.

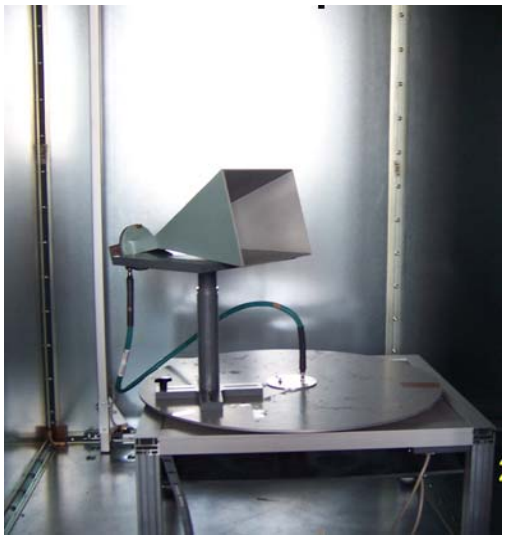

Figure 3.1: Photo of a standard gain horn antenna mounted on the platform in the RC.

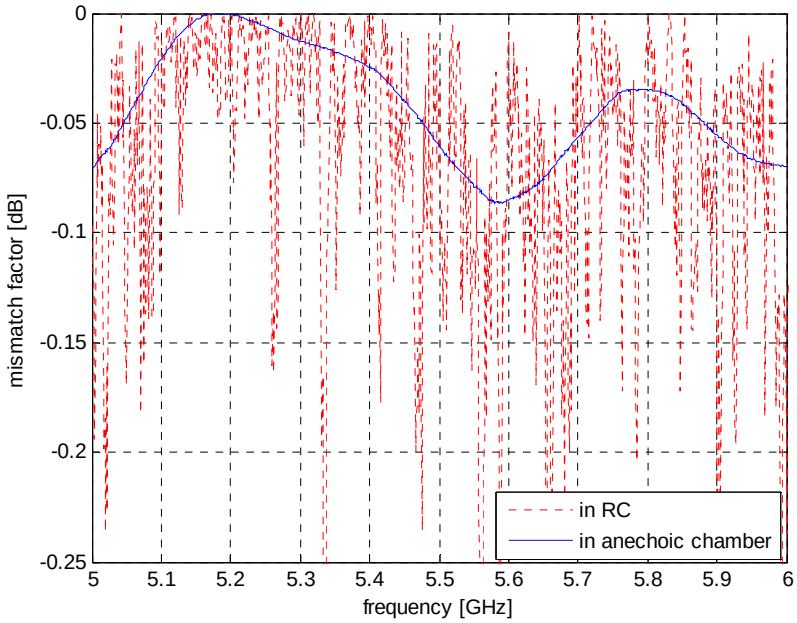

Figure 3.2: Mismatch factor at one stirrer position in RC and in anechoic chamber.

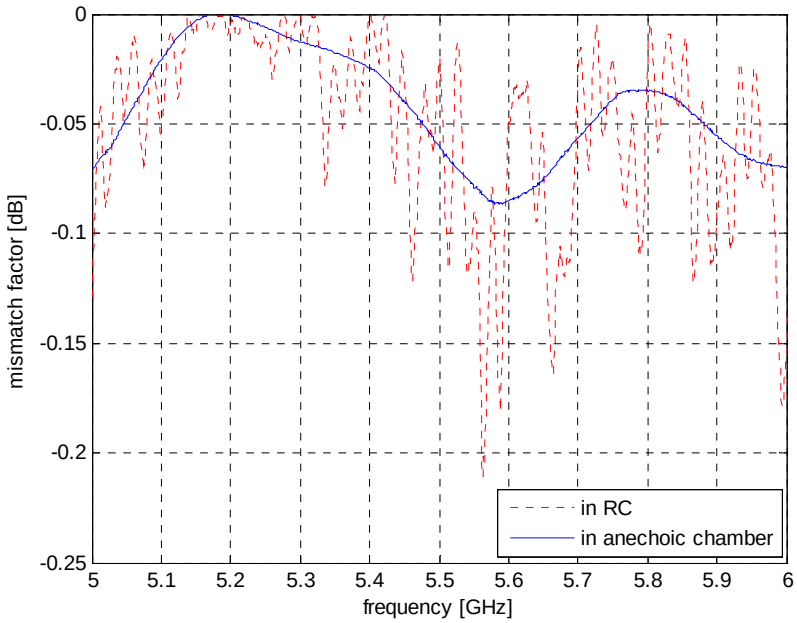

(a)

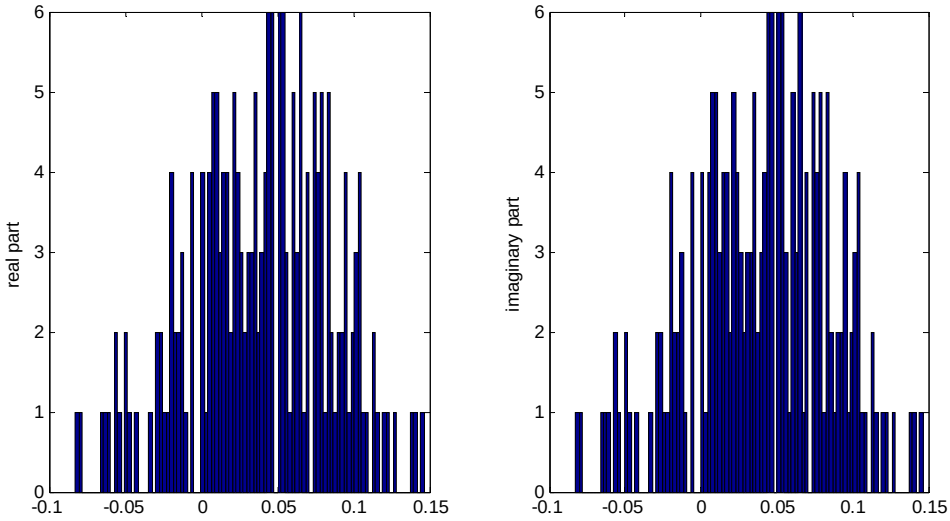

(b)

Figure 3.3: Mismatch factor of AUT in RC with stirrer position average only and that in anechoic chamber (a); histogram of real and imaginary parts of S_{11}^{RC} at 5.5 GHz (b).

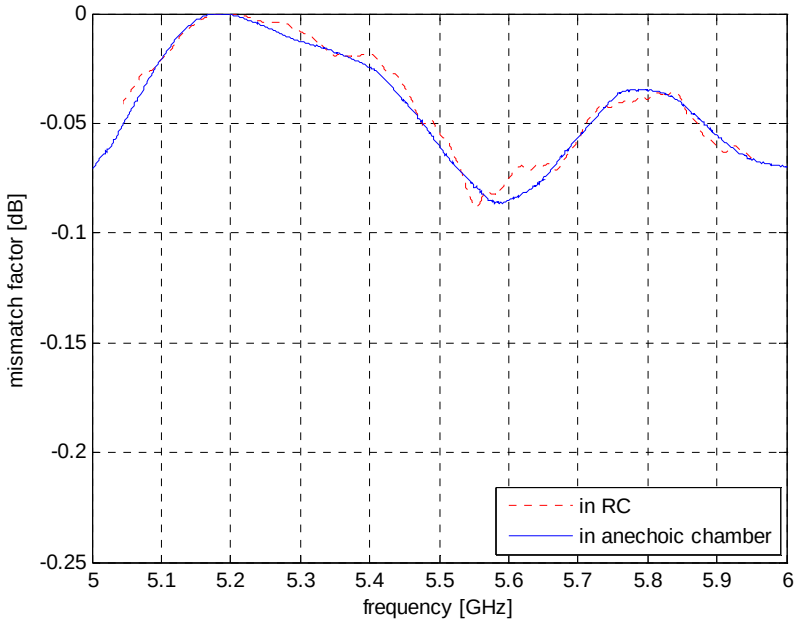

(a)

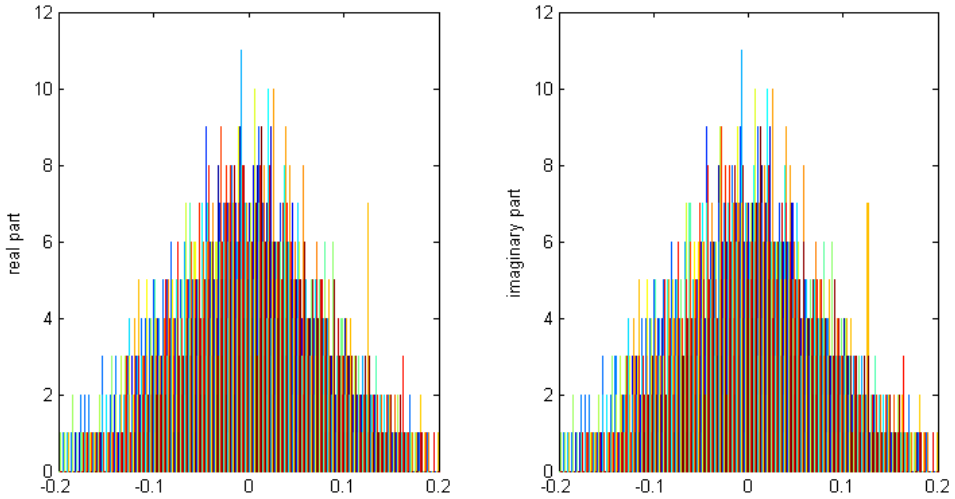

(b)

Figure 3.4: Mismatch factor of AUT measured in reverberation chamber with 100 MHz complex frequency stirring, and that measured in anechoic chamber (a); histogram of real and imaginary parts of S_{11}^{RC} at center frequency 5.5 GHz with a bandwidth of 100 MHz (b).

3.2 Measurement of Diversity Antenna

Application of antenna diversity techniques, most commonly assuming two antennas in the mobile terminal, may reduce the effects of signal fading due to multipath. The general expression for the diversity gain is improved signal-to-noise ratio (SNR) at output of the diversity combiner compared at the input of the diversity antenna at 1% cumulative probability level [36]. Fig. 3.5 illustrates the definition diversity gains. Using selection combining technique, the apparent diversity of a two-port diversity antenna can be approximated by [36]

$$G_{app} \approx 10.48\sqrt{1-|\rho|^2} \tag{3.4}$$

Equation (3.4) assumes equal efficiency for all branches. And it is inaccurate when correlation approaches unity. A more advanced formula that can be used when the branches have different efficiencies and unity correlation can be found in [37]. The effective diversity gain is

$$G_{eff} = e_{emb} G_{App} \tag{3.5}$$

where e_{emb} denotes embedded radiation efficiency. It can be seen from (3.4) and (3.5) that both correlation and embedded radiation efficiency degrade effective diversity gain.

In this thesis we use Eleven antenna [38], which is a multi-port wideband antenna with decade bandwidth, as a two-port diversity antenna [39]. The measurements are done in RC at Chalmers University of Technology (Chalmers) and anechoic chamber (AC) by spherical near-field technique at Technical University of Denmark (DTU), see Fig. 3.6.

The correlation can be calculated based on embedded radiation pattern measured in AC as

$$\rho = \frac{\iint_{4\pi} G_{emb}^{1}(G_{emb}^{2})^{*} d\Omega}{\sqrt{\iint_{4\pi} G_{emb}^{1}(G_{emb}^{1})^{*} d\Omega \cdot \iint_{4\pi} G_{emb}^{2}(G_{emb}^{2})^{*} d\Omega}} \tag{3.6}$$

where G_{emb}^{i} (i=1,2) is the radiation pattern of the ith element while the other element is terminated. The correlation can also be calculated based on the definition of cross-correlation with RC measurements.

$$\rho = \frac{E[V_1 V_2^{*}]}{\sqrt{E[|V_1|^2]E[|V_2|^2]}} \tag{3.7}$$

where V_i (i=1,2) is the complex signal received at ith element port in rich scattering environment. Fig. 3.7 shows the comparison of correlation measured in RC using (3.5) and that in AC using (3.4). Good agreement of correlations measured in RC and AC is observed. Fig. 3.8 compares the apparent diversity gain calculated using (3.4) with RC measured correlation and that obtained based on improved SNR at 1% cumulative probability measured in RC. Fig. 3.9 shows apparent and effective diversity gains obtained based on 1% cumulative probability from RC measurements. The difference between apparent and effective diversity gain is embedded radiation efficiency.

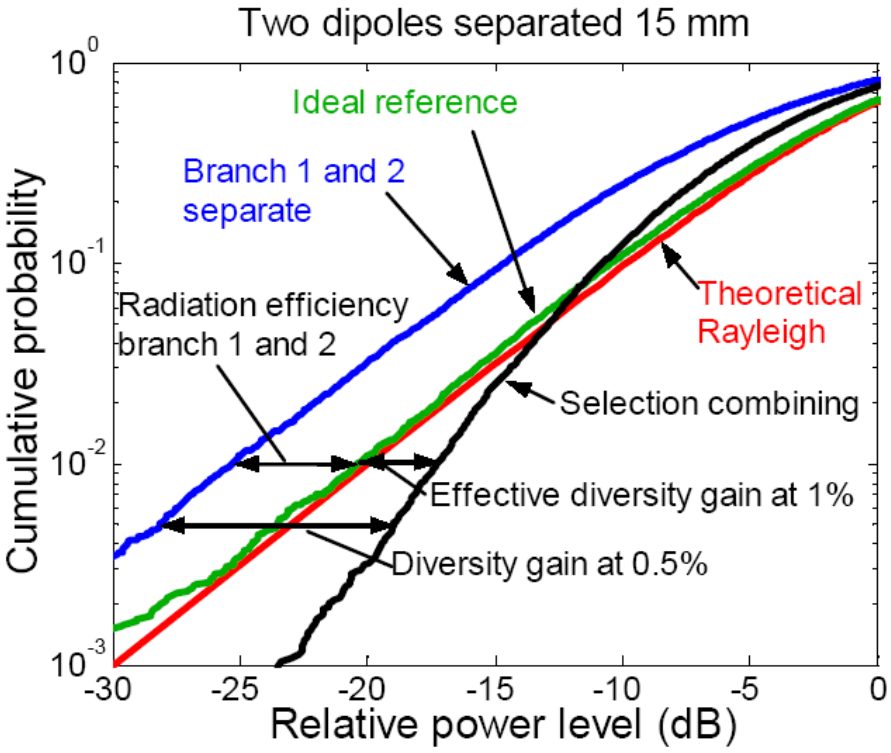

Figure 3.5: Illustration of diversity gains.

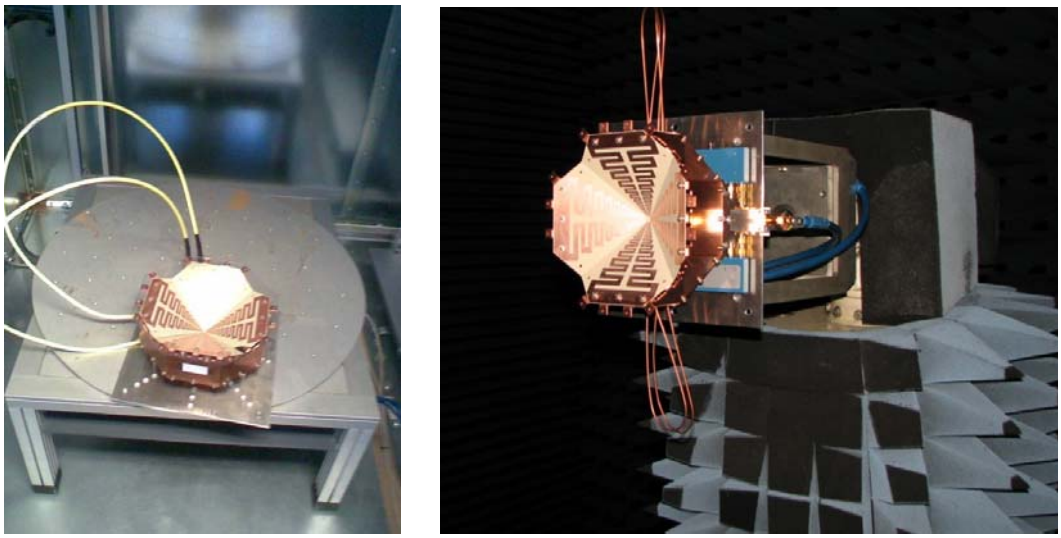

Figure 3.6: Measurement of the Eleven antenna in RC (left) and AC (right).

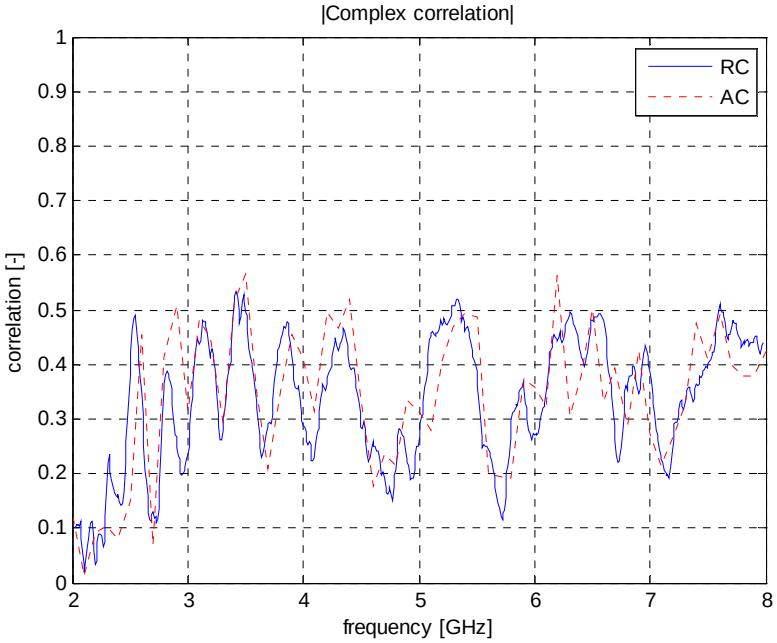

Figure 3.7: Comparison of correlation measured in RC with 20 MHz frequency stirring and that in AC.

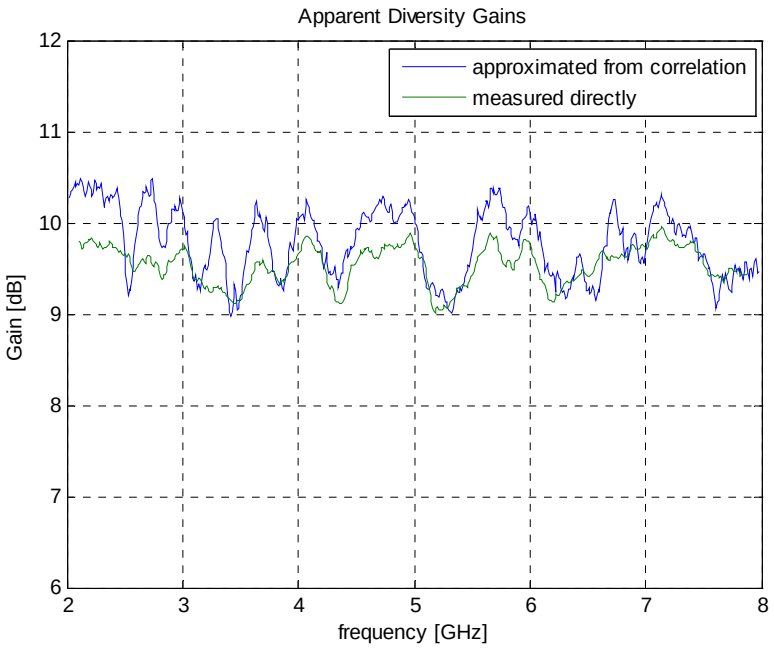

Figure 3.8: Comparison of apparent diversity gain calculated using (3.4) with that obtained based on cumulative probability measured in RC with 20 MHz frequency stirring.

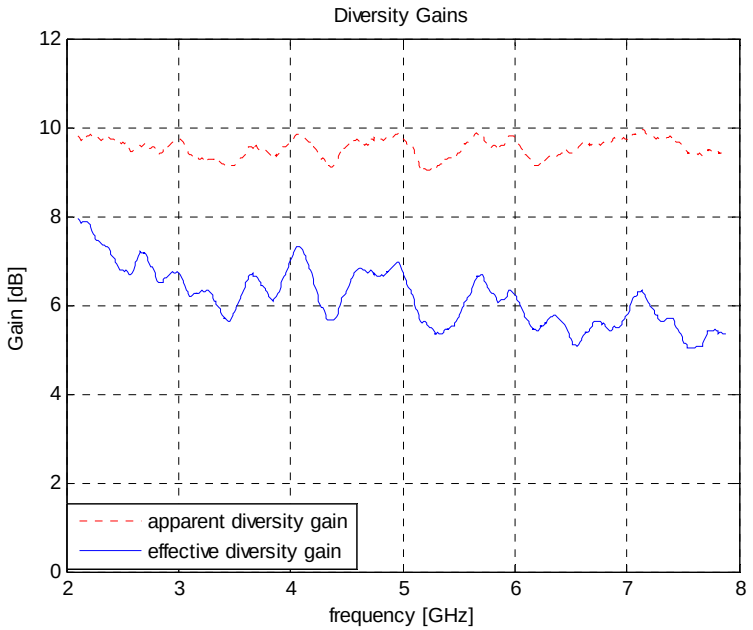

Figure 3.9: Apparent and effective diversity gains measured in RC with 30 MHz frequency stirring.

4. RC Accuracy Characterization

In RC electromagnetic fields can be expanded into orthogonally perturbed mode functions. These perturbed modes satisfy the boundary condition on mode stirrers as well as on cavity walls. The mode stirrers have the effect of shifting the eigen-frequencies and modes, as illustrated in Fig. 4.1 [41]. Fig. 4.1a is 2-D view of the modes (represented by dots) distribution when the mode-stirrer in the RC is stationary, where $k_0 = 2\pi f_0 / c$ is the wave number corresponding to resonant frequency f_0, with speed of light denoted as c. In reality RC always has a finite Q-factor due to different losses [24], corresponding to a non-zero average mode bandwidth Δf [8], [42]. With one single excitation at f_0, all the modes falling within the spherical shell Δk will be excited. Δf is related to the thickness of Δk as $\Delta k = 2\pi\Delta f / c$. With moving mode-stirrer in RC, the eigenmodes start to shift, as shown in Fig. 4.2b. The amount of shift of the eigenmodes depends on the size, geometry and moving sequence of the mode-stirrers. An effective mode-stirrer means the shift of the modes is large enough for modes to shift in and out of the shell. In this way number of independent modes increases. As Wu [41] postulated, the key mechanism behind an effective mode-stirrer lies in the shifting of eigen-frequencies. Therefore, we introduce the concept of mechanical stirring bandwidth to quantify the effectiveness of mode-stirrers.

The well-known Weyl's formula for mode number with frequency band Δf of stationary modes in RC is given as

$$N_m = \frac{8\pi V \Delta f}{\lambda^3 f_0} \tag{4.1}$$

where V is the RC volume, and Δf should be small for (4.1) to hold. Here we denote a Weyl's factor as

$$Weyl = 8\pi V / (\lambda^3 f_0) \tag{4.2}$$

For a RC with stationary mode-stirrers, the maximum independent samples is bounded by

$$N_{ind} = 8 Weyl \Delta f \tag{4.3}$$

where the factor of 8 comes from the fact that almost all the modes can be represented as eight plane waves. As shown in Fig. 4.2b, moving mode-stirrers introduce randomness into the eigenmodes, the effect of which can be accounted by introducing an additional mechanical stirring bandwidth B_{mech}, and the effective shell band becomes $\Delta f + B_{mech}$. Therefore the maximum independent samples in a mode-stirred RC can be expressed as

$$N_{ind} = 8 Weyl (\Delta f + B_{mech}) \tag{4.4}$$

Frequency stirring, has similar effect as mechanical mode stirring [35], and thus can also increase the maximum independent number. However, we will not consider frequency stirring

here, since our main interest is to study the effectiveness of mode-stirrers in RC, and their effects on RC measurement accuracy.

Holloway [18] pointed out that Rican K-factor exists in RC as well. Instead of pointing two directive antennas towards each other to observe K-factor as in [18], we found that K-factor arises even for small nondirective antennas with arbitrary orientations in RC. K-factor here is defined as the ratio of unstirred power to stirred power. In RC unstirred power is the summation of line-of-sight (LOS) power and unstirred multipath (UMP) [18] power. It makes sense since in RC the deterministic UMP has the same effects as LOS. It is shown for the first time in [19] the K-factor represents a residual error of measurement accuracy and the standard deviation (STD) of the power transfer function in RC can be modeled as [19]

$$\sigma = \sqrt{1/N_{ind} + K^2/N_{UMP}} \,/\, \sqrt{1+K^2} \tag{4.5}$$

where N_{UMP} is the number of wall antennas (antennas mounted on walls of the RC) times that of platform positions. STD is finally calculated from nine independent measurements of averaged power transfer functions at each frequency. In this thesis, STD σ is presented in dB scale by averaging the dB values of $(1+\sigma)$ and $(1-\sigma)$ where σ is the actual STD of the measured quantity,

$$\sigma_{dB} = 5\log[(1+\sigma)/(1-\sigma)] \tag{4.6}$$

In order to measure the STD as a function of frequency, we did nine measurements by putting the reference antenna in three heights and three orientations (horizontal, vertical and 45 degree tilted) at each height. At each reference antenna position/orientation there are certain mode-stirrer (including platform) samples depending on the stirring sequence, from which we can calculate the averaged power transfer function. STD is finally calculated from the nine averaged power transfer functions at each frequency. This procedure is repeated for 5 different RC loadings. The loadings are specified as: *load0* corresponds to unloaded RC, *load1* is a head phantom filled with brain equivalent liquid in terms of microwave absorption, *load2* is the head phantom plus three Polyvinyl Chloride (PVC) cylinders filled with microwave absorbers, *load3* is the head phantom plus six such cylinders, and *load4* is the head phantom plus nine cylinders. The lossy cylinders were located along orthogonal corners of the chamber in such a way that they can be expected to attenuate cavity modes of different polarizations equally much (TE and TM modes).

K-factor, *K*, in (4.5) can be obtained from S-parameters

$$K = \left|\overline{S_{21}}\right|^2 / \left|\overline{S_{21} - \overline{S_{21}}}\right|^2 \tag{4.7}$$

where the overhead bar represents complex mean operator. The average mode bandwidth is given in (2.5). The mechanical stirring bandwidth is taken as an empirical value of 3 MHz for the mode-stirrers in Bluetest RC. The platform is rotated to 20 positions spaced by 18 degree, and for each platform position each of the two stirrer-plates move simultaneously to 50 positions, each distributed evenly along the total distances they can move. At each stirrer position and for each of the three wall antennas, a full frequency sweep is performed by the VNA. K-factors calculated at different RC loadings are shown in Fig. 4.2, from which it is seen that K-factor increases with increasing lossy objects. Note that the different frequency-

dependency of K-factor in this thesis and that in [18] is due to the fact that the latter pointed two directive antennas towards each other, while K-factor measured here is for small nondirective antennas with arbitrary orientations in RC.

Based on measured K-factor and average mode bandwidth, the measured STDs are plotted against the accuracy model predicted values using (4.5). From Fig. 4.3 one can see the accuracy model predict measurements better for high frequencies. It is because the RC works properly above 800 MHz; below that the RC does not support as many modes, and thereby introduces more uncertainty. Anyway, it can be seen that the accuracy model offers a good prediction of the measurement accuracy trend as a function of frequency for different loadings.

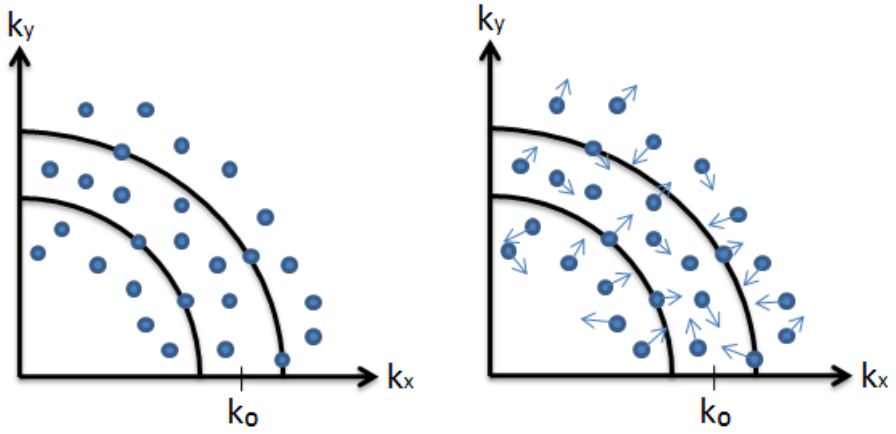

(a) (b)

Figure 4.1: Mode distribution near resonating frequency in RC: (a) stationary mode-stirrer; (b) moving mode-stirrer.

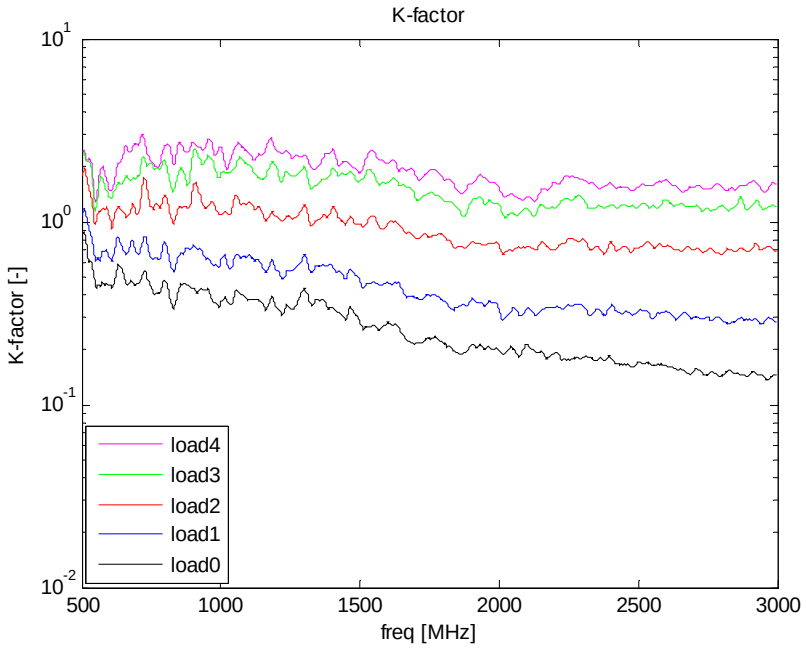

Figure 4.2: Measured K-factor in RC at different loadings, for each loading it is averaged over the nine independent measurements plus 20MHz frequency smoothing.

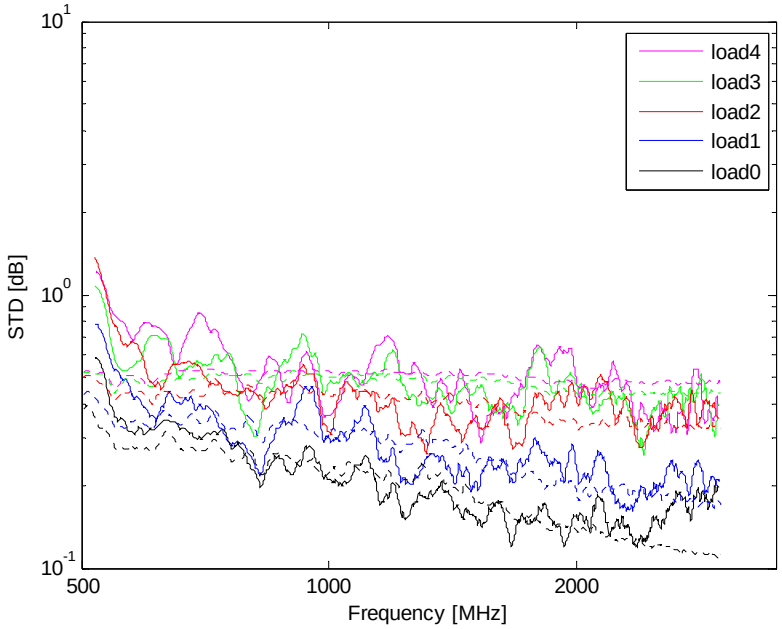

Figure 4.3: Measured STD in RC with 50MHz frequency smoothing against theoretical model.

5. Conclusions

In this thesis RC is characterized for various OTA measurements.

For applications of active OTA measurements, channel sounding is performed to determine coherence bandwidth, delay spread and Doppler spread. It is found that coherence bandwidth and average mode bandwidth are the same, and RMS delay spread is proportional to decay time in RC. While average mode bandwidth and decay time in RC can be easily calculated, they turn out to be computationally cheaper alternative for time-dispersive channel sounding. More importantly, it is found that channel can be controlled (flat or frequency-selective) by simply loading the RC. In addition, a novel method to determine Doppler spread using step-wise stationary stirring is presented. With this method, one can determine Doppler spread for any frequency within the sweeping frequency band at the same time; and Doppler spreads corresponding to different speeds can be obtained simply by a scaling factor.

It is shown that RC can be used to measure radiation efficiency and mismatch factor of single-port antenna, and diversity for multi-port antennas. It is shown that with certain complex frequency stirring free space reflection coefficient of antennas can be predict in RC with very good accuracy. It is also shown that correlation and diversity gains of multi-port antenna can be estimated accurately in RC. Compared with AC measurement, RC measurement requires less time. Moreover, RC is much cheaper than AC.

For both active and passive OTA measurements, accuracy of RC measurement is of important. In this thesis, we characterized RC measurement accuracy in terms STD as a function of frequency. In addition, an RC accuracy model is presented. It is shown that the accuracy model can be used to predict measured STD well.

References

[1] J. G. Kostas and B. Boverie, "Statistical model for a mode-stirred chamber," *IEEE trans. Electromagn. Compat.,*vol.33, no. 4, pp. 366-370*,* Nov. 1991.

[2] K. Rosengren and P.-S. Kildal, "Radiation efficiency, correlation, diversity gain and capacity of a six-monopole antenna array for a MIMO system: theory, simulation and measurement in reverberation chamber," *IEE Proc. Microw. Antennas Propag.* vol. 152, pp. 7-16, 2005. See also Erratum published in August 2006.

[3] N. Serafimov, P-S. Kildal, T. Bolin, "Comparison between radiation efficiencies of phone antennas and radiated power of mobile phones measured in anechoic chambers and reverberation chamber", *IEEE AP-S International Symposium*, San Antonio, Texas, June 2002.

[4] C. Orlenius, P.–S. Kildal, and G. Poilasne, "Measurement of Total Isotropic Sensitivity and Average Fading Sensitivity of CDMA phones in Reverberation Chamber," *IEEE AP-S Internal Symp. Washington D.C.,* 3-8 July*,* 2005.

[5] K. Rosengren, Characterization of terminal Antennas for diversity and MIMO systems by theory, simulations and measurements in reverberation chamber, PhD thesis at Chalmers University of Technology, 2005.

[6] K. Rosengren and P.-S. Kildal, "Study of distribution of modes and plane waves in reverberation chambers for the characterization of antennas in a multipath environments," *Microwave and optical technology letters*, vol. 30, no. 6, pp. 386-391, Sep. 2001.

[7] D. A. Hill, "Linear dipole response in a reverberation chamber," *IEEE trans. Electromagn. Compat.,* vol.41, no. 4, pp. 365-368*,* Nov. 1999.

[8] X. Chen, P.-S. Kildal, C. Orlenius, J. Carlsson, "Channel sounding of loaded reverberation chamber for Over-the-Air testing of wireless devices - coherence bandwidth and delay spread versus average mode bandwidth", *IEEE Antennas and Wireless Propagation Letters*, vol. 8, pp. 678-681, 2009.

[9] Xiaoming Chen, Per-Simon Kildal, "Theoretical derivation and measurements of the relationship between coherence bandwidth and RMS delay spread in reverberation chamber", EuCAP 2009, March 2009.

[10] Xiaoming Chen, Per-Simon Kildal, "Comparison of RMS Delay Spread and Decay Time Measured in Reverberation Chamber", EuCAP 2010, Barcelona, Spain April 2010.

[11] K. Karlsson, X. Chen, P.-S. Kildal and J. Carlsson, "Doppler spread in reverberation chamber predicted from measurements during step-wise stationary stirring", *IEEE Antennas and Wireless Propagation Letters*, vol. 9, pp. 497-500, 2010.

[12] Xiaoming Chen, Per-Simon Kildal, "Accuracy of antenna mismatch factor and input reflection coefficient measured in reverberation chamber", EuCAP 2009, 23-27 March, Berlin, Germany, 2009.

[13] Jian Yang, Xiaoming Chen, Niklas Wadefalk, Per-Simon Kildal, "Design and realization of a linearly polarized Eleven feed for 1-10 GHz", *IEEE Antennas and Wireless Propagation letters*, vol.8, pp. 64-68. 2009.

[14] A.A.H. Azremi, J. Toivanen, T. Laitinen, P. Vainikainen, X. Chen, N. Jamaly, J. Carlsson, P.-S Kildal, S. Pivnenk, "On Diversity Performance of Two-Element Coupling Element Based Antenna Structure for Mobile Terminal", EuCAP 2010, Barcelona, Spain, 2010.

[15] J. Yang, S. Pivnenko, T. Laitinen, J. Carlsson, X. Chen, "Measurements of Diversity Gain and Radiation Efficiency of the Eleven Antenna by sing Different Measurement Techniques,", EuCAP 2010, Barcelona, Spain, 2010.
[16] Y. B. Karandikar, D. Nyberg, N. Jamaly, P.-S. Kildal, "Mode counting in rectangular, cylindrical and spherical cavities with application to wireless measurements in reverberation chambers," *IEEE trans. Electromagn. Compat.,*vol. 51, no. 4, pp. 1044-1046, Nov. 2009.
[17] Xiaoming Chen, Per-Simon Kildal, "Frequency-Dependent Effects of Platform and Wall Antenna Stirring on Measurement Uncertainty in Reverberation Chamber", EuCAP 2010, Barcelona, Spain, 12-16 April 2010.
[18] C. L. Holloway, D. A. Hill, J. M. Ladbury, P. F. Wilson, G. Koepke, and J. Coder, "On the Use of Reverberation Chamber to Simulate a Rician Radio Environment for the Testing of Wireless Devices," *IEEE Trans. on Antennas and Propagation, vol. 54, No. 11*, pp. 3167-3177, Nov. 2006.
[19] Per-Simon Kildal, Sz-Hau Lai, and Xiaoming Chen, "Direct Coupling as a Residual Error Contribution during OTA Measurements of Wireless Devices in Reverberation Chamber", IEEE AP-S, Charleston, USA, June 1-5, 2009.
[20] W.C. Jakes, Microwave Mobile Communications. 2nd ed., Wiley, 1994.
[21] M. J. Gans, "A power-spectral theory of propagation in the mobile-radio environment," *IEEE Trans. Vechicular Tech.,* vol. 21, no. 1, Feb. 1972.
[22] G. J. M. Janssen, P. A. Stigter, and R. Prasad, "Wideband Indoor Channel Measurements and BER Analysis of Frequency Selective Multipath Channels at 2.4, 4.75, and 11.5 GHz," *IEEE Trans. on communications,* vol. 44, no. 10, pp. 1272-1288, Oct. 1996.
[23] T. S. Rappaport, *Wireless Communications—Principles and Practice*. 2nd ed., Prentice Hall PTR, 2002, pp.196-202.
[24] D. A. Hill, M. T. Ma, A. R. Ondrejka, B. F. Riddle, M. L. Crawford, and R. T. Johnk, "Aperture Excitation of Electrically Large, Lossy Cavities," *IEEE trans. Electromagn. Compat.,vol.36, no. 3,pp169-178,* Aug. 1994.
[25] K. Rosengren, P-S. Kildal, C. Carlsson, J. Carlsson, "Characterization of Antennas for Mobile and Wireless Terminals in Reverberation Chambers: Improved Accuracy by Platform Stirring", *Microwave and Optical Technology Letters,* Vol. 30, No 20, pp 391-397, Sep. 2001.
[26] P-S. Kildal, C. Carlsson, "Detection of a polarization imbalance in reverberation chambers and how to remove it by polarization stirring when measuring antenna efficiencies", Microwave and Optical Technology Letters, Vol. 32, No 2, pp. 145-149, July 20, 2002.
[27] A. Goldsmith, *Wireless Communications*, Cambridge university press, 2005.
[28] S. Stein, "Fading channel issues in system engineering," *IEEE Journal on selected areas in communications*, vol. 5, no. 2, pp. 68-89, Feb. 1987.
[29] S. J. Howard, K. Pahlavan, "Doppler spread measurement of indoor radio channel," *Electronic letters*, vol. 26, no. 2, pp. 107-109, Jan. 1990.
[30] Mehrez Souden, Sofiène Affes, Jacob Benesty, and Rim Bahroun, "Robust Doppler Spread Estimation in the Presence of a Residual Carrier Frequency Offset," *IEEE Trans. on signal processing*, vol. 57, no. 10, Oct. 2009.
[31] P. Hallbjörner, A. Rydberg, "Maximum Doppler frequency in reverberation chamber with continuously moving stirrer," *Loughborough antenna and propagation conference*, 2007.
[32] Y. Huang, R. M. Narayanan and G. R. Kadambi, "Electromagnetic coupling effects on the cavity measurement of antenna efficiency," *IEEE trans. on Antennas and Propagation ,*vol. 51, no. 11, pp. 30647-3071, Nov. 2003.

[33] L. K. Warne, K. S. H. Lee, H. G. Hudson, W. A. Johnson, R. E. Jorgenson and S. L. Stronach, “Statistical properties of linear antenna impedance in an electrically large cavity,” *IEEE trans. on Antennas and Propagation ,*vol. 51, no. 5, pp. 978-992, May. 2003.
[34] P. -S. Kildal, C. Carlsson and J. Yang, “Measurement of free-space impedance of small antennas in reverberation chamber,” *Microwave and optical tech. letters,* vol. 32, no. 2, pp. 112-115, Jan. 20, 2002.
[35] D. A. Hill, “Electronic mode stirring for reverberation chamber,” *IEEE trans. Electromagn. Compat.,*vol. 36, no. 4, pp. 294-299, Nov. 1994.
[36] P-S. Kildal, K. Rosengren, “Electromagnetic analysis of effective and apparent diversity gain of two parallel dipoles”, *IEEE Antennas and Wireless Propagation Letters*, Vol. 2, No. 1, pp 9-13, 2003.
[37] N. Jamaly, P.-S. Kildal, J. Carlsson, “Compact formulas for diversity gain of two-port antennas”, submitted to *IEEE Antennas and Wireless Propagation Letters*, 2010.
[38] Jian Yang, Xiaoming Chen, Niklas Wadefalk, Per-Simon Kildal, "Design and realization of a linearly polarized Eleven feed for 1-10 GHz", *IEEE Antennas and Wireless Propagation letters*, vol.8, pp. 64-68. 2009.
[39] J. Yang, S. Pivnenko, T. Laitinen, J. Carlsson, X. Chen, “Measurements of Diversity Gain and Radiation Efficiency of the Eleven Antenna by sing Different Measurement Techniques,”, EuCAP 2010, Barcelona, Spain, 2010.
[40] X. Chen, N. Jamaly, J. Carlsson, J. Yang, P.-S. Kildal, A. Hussain, “Comparison of Diversity Gains of Wideband Antennas Measured in Anechoic and Reverberation Chambers”, GigaHertz Symposium 2010, Lund, 9-10, March 2010.
[41] D. I. Wu and D. C. Chang, “The effect of an electrically large stirrer in a mode-stirred chamber,” *IEEE trans. Electromagn. Compat.,vol.31, no. 2,pp164-169,* May. 1989.
[42] U. Carlberg, P.-S. Kildal, and J. Carlsson, “Study of antennas in reverberation chamber using method of moments with cavity Green’s function calculated by Ewald summation,” *IEEE Trans. Electromagn. Compat.*, vol. 47, no.4, pp. 805-814, Nov. 2005.